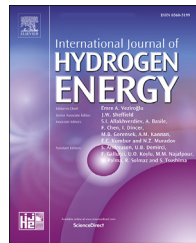




ELSEVIER

Available online at www.sciencedirect.com**ScienceDirect**journal homepage: www.elsevier.com/locate/he

Experimental study of premixed syngas/air flame deflagration in a closed duct

Minggao Yu ^{a,b}, Xufeng Yang ^a, Kai Zheng ^{a,*}, Ligang Zheng ^b,
Xiaoping Wen ^c

^a State Key Laboratory of Coal Mine Disaster Dynamics and Control, Chongqing University, Chongqing 400044, PR China

^b School of Safety Science and Engineering, Henan Polytechnic University, Jiaozuo 454003, PR China

^c School of Mechanical and Power Engineering, Henan Polytechnic University, Jiaozuo 454003, PR China

ARTICLE INFO

Article history:

Received 6 April 2018

Received in revised form

15 May 2018

Accepted 16 May 2018

Available online 6 June 2018

Keywords:

Syngas/air

Premixed flame

Tulip flame

Distorted tulip flame

Flame oscillation

ABSTRACT

The propagation behaviour of a deflagration premixed syngas/air flame over a wide range of equivalence ratios is investigated experimentally in a closed rectangular duct using a high-speed camera and pressure transducer. The syngas hydrogen volume fraction, φ , ranges from 0.1 to 0.9. The flame propagation parameters such as flame structure, propagation time, velocity and overpressure are obtained from the experiment. The effects of the equivalence ratio and hydrogen fraction on flame propagation behaviour are examined. The results indicate that the hydrogen fraction in a syngas mixture greatly influences the flame propagation behaviour. When φ , the hydrogen fraction, is ≥ 0.5 , the prominently distorted tulip flame can be formed in all equivalence ratios, and the minimum propagation time can be obtained at an equivalence ratio of 2.0. When $\varphi < 0.5$, the tulip flame distortion only occurs in a hydrogen fraction of $\varphi = 0.3$ with an equivalence ratio of 1.5 and above. The minimum flame propagation time can be acquired at an equivalence ratio of 1.5. The distortion occurs when the maximum flame propagation velocity is larger than 31.27 m s^{-1} . The observable oscillation and stepped rise in the overpressure trajectory indicate that the pressure wave plays an important role in the syngas/air deflagration. The initial tulip distortion time and the plane flame formation time share the same tendency in all equivalence ratios, and the time interval between them is nearly constant, 4.03 ms. This parameter is important for exploring the quantitative theory or models of distorted tulip flames.

© 2018 Hydrogen Energy Publications LLC. Published by Elsevier Ltd. All rights reserved.

Introduction

Synthesis gas, also known as syngas, primarily consists of hydrogen and carbon monoxide as well as a small amount of methane, carbon dioxide, nitrogen and water, and it can be

produced from various sources, such as coal, biomass, refinery bottom residues, and municipal waste [1–6]. Syngas combustion can result in a significant reduction of pollutant emissions such as SO_x , NO_x , particulates, and heavy metals, and a potential reduction in carbon dioxide using carbon

* Corresponding author. 174 Shazhengjie, Shapingba, Chongqing, 400030, China.

E-mail address: zkcqu@cqu.edu.cn (K. Zheng).

<https://doi.org/10.1016/j.ijhydene.2018.05.103>

0360-3199/© 2018 Hydrogen Energy Publications LLC. Published by Elsevier Ltd. All rights reserved.

capture and sequestration (CCS) technology. Syngas is attracting increasing interest as an environmentally friendly renewable energy that is currently used in the integrated gasification combined cycle (IGCC) power plant [7]. However, the changeable hydrogen and carbon monoxide content, which may be caused by various gasification methodologies and source quality [8], is one of the largest barriers to the extensive use of syngas. The variability of syngas composition has a significant influence on the combustion and explosion characteristics, making the prevention of syngas explosions more difficult [9–11]. Important and basic flame parameters are essential to the safe utilization of syngas.

The premixed combustion of syngas has been widely investigated in past decades [12–22], but experiments on premixed syngas/air flames in a closed duct are quite limited. The premixed flame in a closed duct is one of the important aspects of syngas premixed combustion to explore. During flame propagation in a closed duct, many factors can affect the flame such as body force, boundary layers and intrinsic instabilities (Rayleigh-Taylor, Richtmyer-Meshkov and Darrieus-Landau) [23,24], making the flame structure and shape more complicated. Flame structure is a crucial parameter for characterizing flame behaviour, and it explains the flame propagation mechanism. Flame propagation in a closed duct can undergo a series of structural and shape changes under the appropriate conditions. Among all the flame shapes, the most attractive and interesting one is the tulip shape. A tulip flame was first observed by Ellis in 1928 [25] and subsequently named by Salamandra in 1959 [26]. The tulip phenomenon has been described in numerous experimental and numerical studies [27–29]. The four essential phases of a tulip flame are the following: (a) a hemispherical flame; (b) a finger-shaped flame; (c) an elongated flame with flame skirts touching the sidewalls; and (d) a tulip flame.

The tulip flame phenomenon puzzles many researchers in the domain of premixed combustion because it can be affected by many factors. Various hypotheses have been proposed to explain the tulip flame formation process, e.g., quenching and viscosity effects [25,30], vortex motion effects [31–33], pressure wave effects [34], Darrieus-Landau (DL) instability effects [35–38] and the Taylor instability effect [39], but none is certain. Xiao et al. [40] suggest that the formation of a tulip flame is a multi-factor interaction. Moreover, external conditions can affect the tulip flame formation. The tulip phenomenon is very sensitive to the aspect ratio. The tulip flame is obtained only in a closed duct with an aspect ratio of >2.0 [25], and it will form only in a half-open duct with an aspect ratio of >6.7 [41]. In addition, the combustible gas has significant influence on flame structure and shape. The flame will undergo a more drastic structure change in highly reactive gas such as hydrogen. Recently, a remarkable tulip flame distortion phenomenon in a premixed hydrogen/air flame was revealed by Xiao et al. who suggests the distorted tulip flame is an additional stage on the premixed flame [42,43]. The pressure wave triggered by the flame touching the sidewall is responsible for the periodic shape change. Rayleigh-Taylor instability plays an important role in distorted tulip flame formation [40,44,45]. The distorted tulip flame is not a unique phenomenon in premixed hydrogen/air flames, and it can also be obtained in premixed acetylene/air,

propane/air and methane/hydrogen/air flames [46–49]. However, there are still insufficient data to make the distorted tulip flame formation explanation more convincing.

Although a large number of studies have been conducted to qualitatively reveal the mechanism of the tulip flame and distorted tulip flame formation, additional information is still required regarding a quantitative theory or model to predict the tulip flame and distorted tulip flame. Several analytical theories have been explored to quantitatively predict tulip flame formation [28,50], but these theories only work well in specific conditions. At the distorted tulip flame stage, a quantitative model is missing. Thus, more premixed flame data should be obtained for full consideration. Additionally, there is a lack of studies characterizing syngas explosion flame propagation and pressure dynamics in different scenarios. To address the safety issues of syngas combustion, it is of the utmost importance to study the flame characteristics of premixed syngas/air mixtures over wide range of mixture compositions.

In this study, a systematic investigation of premixed syngas/air mixture flame characteristics is conducted in a closed rectangular duct over a wide range of equivalence ratios and mixture compositions. Through high-speed camera image processing, the syngas explosion flame structure and velocity are obtained. Meanwhile, the pressure dynamics are acquired by a pressure transducer. The flame characteristics of premixed syngas/air mixtures are specially scrutinized. This work can provide more knowledge for premixed flame dynamics and contribute to safe industrial designs.

Experimental setup

The experimental setup is schematically shown in Fig. 1. The system consists of a combustion chamber, a gas distribution system, an ignition system and a data acquisition system. A high-transparency rectangular Plexiglas duct with an inner cross-section of 100 × 100 mm is employed as the combustion chamber. The length of the duct is 1000 mm to ensure the full formation of the remarkable curved tulip flame [24]. Both ends of the duct are closed with TP304 stainless steel plates. There is a round discharge vent near the right end of the duct with the inner diameter of 30.293 mm. The discharge vent is closed by the PVC membrane, and it breaks up easily for safety's sake. The premixed syngas/air mixture is prepared by the partial pressure method. The flow rate of each gas is precisely monitored with three scientific mass flow controllers (Alicat M) to provide the desired mixture composition. When the inlet gas is four times the volume of the rectangular duct, the syngas/air is fully mixed [41].

The mixture is ignited by a pair of spark electrodes with a 2 mm gap perpendicular to the duct axis. The spark electrodes are located in the left stainless steel plate at the centre of the cross-section. For collecting the dynamic pressure details in the duct, the pressure is measured by an MD-HF piezoelectric gauge pressure transducer from Shanghai Mingkong Sensor Technology Co., Ltd. The pressure transducer is located in the stainless plate 20 mm away from the spark electrode. In addition, an FS-N18 N photoelectric transducer is used to record the ignition time. The data acquisition frequency of the

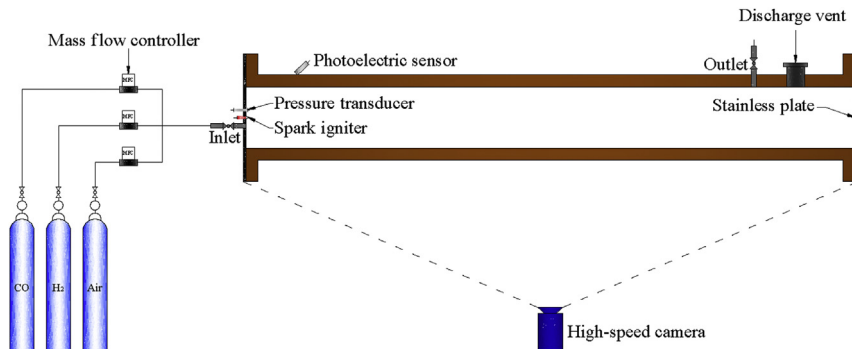


Fig. 1 – Sketch of experimental setup.

pressure transducer and the photodiode sensor are 15 kHz. The flame propagation structural evolution is captured graphically at 3200 frame/s with a “Phantom” high-speed camera (Phantom Miro M310).

Experiments are conducted with premixed syngas/air mixtures at various equivalence ratios and hydrogen fractions. The equivalence ratio, ϕ , is defined as Eq. (1), and the hydrogen fraction, φ , is defined as Eq. (2), as follows:

$$\phi = \frac{(F/A)}{(F/A)_{\text{Stoch}}} \quad (1)$$

$$\varphi = \frac{V_{H_2}}{V_{H_2} + V_{CO}} \quad (2)$$

where (F/A) and $(F/A)_{\text{Stoch}}$ are the actual fuel/air and the stoichiometric fuel/air ratios, respectively; and V_{H_2} and V_{CO} represent the volumes of hydrogen and carbon monoxide, respectively. It should be noted that the purities of hydrogen and carbon monoxide are 99.995% and 99.99%, respectively. All the experiments are carried out at initial atmospheric temperature and pressure. Each test is repeated at least three times to ensure reliable results.

Results and discussion

Flame structure characteristics and change

Generally, flame propagation in a duct with a width that is much larger than the flame thickness can undergo a series of structural changes [24]. The typical flame structural evolution

along the duct is the process of tulip flame formation. Fig. 2 shows the equivalence ratio of flame structural evolution is 1.0 and hydrogen fraction is 0.9. After ignition, the flame expands freely as a hemispherical shape that is unaffected by the sidewalls, as seen at $t = 1.24$ ms. As the flame moves on, the lateral expansion will be confined by the sidewalls, the hemispherical flame will be stretched into a finger shape (see $t = 4.34$ ms), and the flame surface area will be increased exponentially in time [50]. At approximately $t = 6.51$ ms, the flame skirts begin touching the sidewalls. Then, the flame surface area decreases drastically, and a plane flame forms at $t = 8.99$ ms. The tulip flame, which is defined as a curved flame from the unburned to the burned field, can be clearly distinguished between $t = 9.61$ and $t = 10.85$ ms. Furthermore, there is a distortion on the tulip lips after the classical tulip flame formation. The first distortion with a secondary cusp on the classical tulip lips starts at approximately $t = 13.02$ ms. The distortion becomes remarkable with the flame propagation along the duct. The distorted tulip flame shape, which is defined as an additional phase by Xiao et al. [42,43], can be subsequently obtained at $t = 13.64, 13.95, 14.57$, and 15.19 ms. When $t > 16.74$ ms, the distorted tulip flame disappears and then develops into a secondary distorted tulip flame, and this process repeats until the flame leading tip arrives at the discharge vent [40,42–45,51].

The images in Fig. 3 give the structural evolution of syngas/air premixed flames with various hydrogen fractions and equivalence ratios. The contrast and luminosity have been treated to better expose the flame structure in Fig. 3(d) and (e) with $\varphi = 0.9$. As shown in Fig. 3, one can clearly distinguish the four phases of tulip flame as mentioned above (The

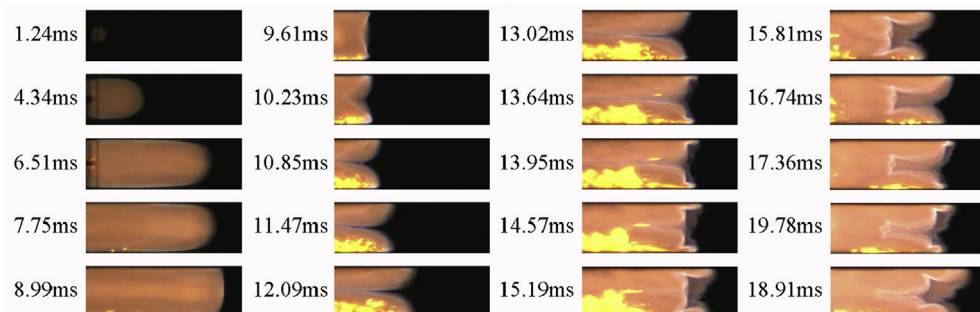


Fig. 2 – High-speed images of premixed syngas/air flame at $\phi = 1.0$ and $\varphi = 0.9$.

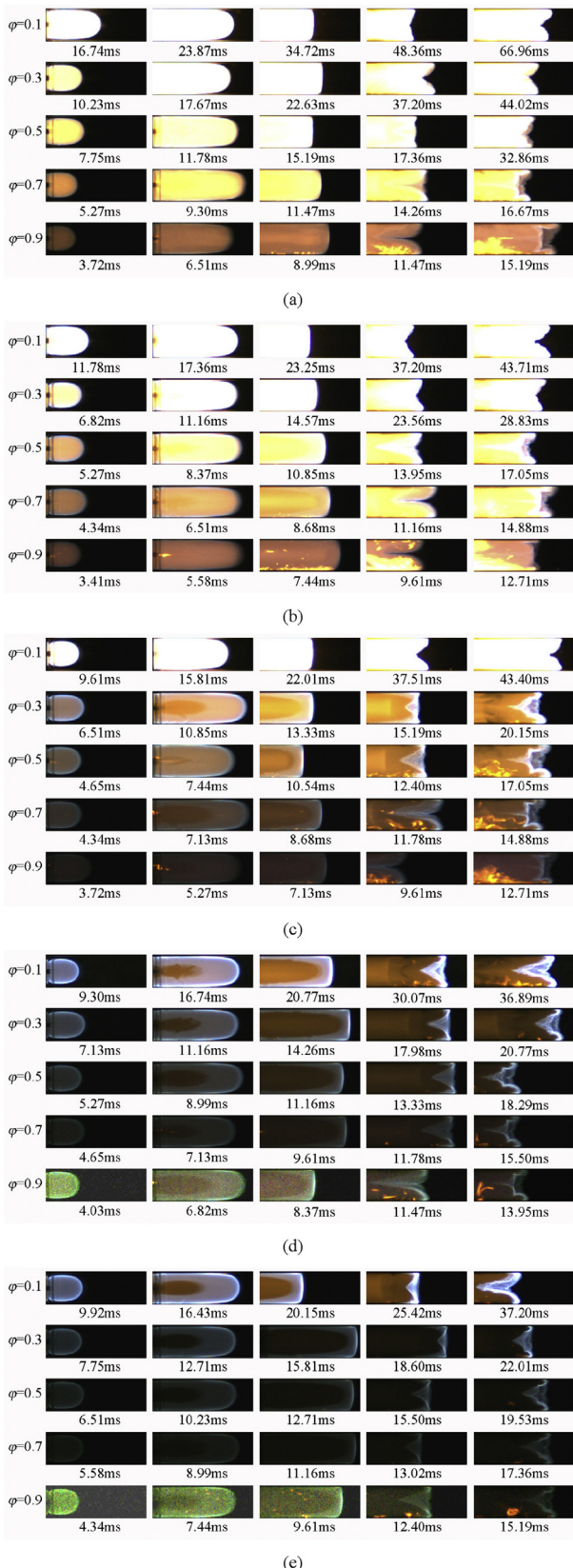


Fig. 3 – High-speed images of premixed syngas/air flames. (a) $\Phi = 1.0$, (b) $\Phi = 1.5$, (c) $\Phi = 2.0$, (d) $\Phi = 2.5$, (e) $\Phi = 3.0$.

hemispherical flame is absent in Fig. 3). The classical tulip flame forms at all equivalence ratios and hydrogen fractions. The distorted tulip flame, however, can be obtained in most of the cases. When the hydrogen fraction is $\varphi \geq 0.5$, the distorted tulip flame can be clearly distinguished at all equivalence ratios. As shown in Fig. 3(a), the distortion in hydrogen fraction of 0.5 is indistinct because of the significant brightness of the flame surface. More details of this situation will be discussed in the flame and pressure dynamics section. It is difficult to identify the distorted tulip flame when the hydrogen fraction is lower than 0.5 ($\varphi < 0.5$). Apparently, the distortion occurs at equivalence ratios of 1.5 and above with a hydrogen fraction of 0.3, as seen in Fig. 3. For an equivalence ratio of 1.5 and hydrogen fraction of 0.3, a small cusp, which is the same as the numerical results in Ref. [52], can be observed on the tulip lips (see $t = 28.83$ ms in Fig. 3(b)). In the other cases, the flame just propagates as the tulip shape to the end of the duct.

The premixed syngas/air flame structure and shape are significantly affected by the hydrogen fraction in the syngas mixture. The tulip flame shape is more cusped as the hydrogen fraction increases. In other words, the tulip lips will become much more elongated, as seen in Fig. 3(b) of $\varphi = 0.1$ at $t = 37.20$ ms and $\varphi = 0.9$ at $t = 9.61$ ms. Meanwhile, the distortion becomes more remarkable as the hydrogen fraction increases. Note that the flame propagates with a quite smooth surface before the plane flame formation, whereas the flame surface is progressively wrinkled after inversion. Hydrodynamic instability may be responsible for flame wrinkling because the effective Lewis number of the syngas/air mixture is greater than 1.0 [14], and the flame can be stabilized by thermal-diffusion effects. The flame wrinkling becomes more prominent at an equivalence ratio of 2.0 and above. There is, however, a great disparity of laminar flame speed at rich conditions ($\varphi \geq 2.0$) according to a number of studies [8,12–18]. This disparity has been explained by the authors' different approaches and experimental methods by the authors and by the unwanted carbonyl compounds in syngas combustion [17,53]. Besides, the great discrepancy of reactivity and diffusivity between hydrogen and carbon monoxide may cause unstable combustion of the syngas/air mixture. There is a competition between hydrogen and carbon monoxide in rich conditions because of limited oxygen content in air. This competition could result in unstable syngas combustion that can be amplified after the flame inversion, especially at an equivalence ratio of 2.0 and above.

Flame tip characteristics and pressure dynamics

Figs. 4 and 5 display the locations and velocities of the flame leading tips under various equivalence ratios and hydrogen fractions, and all obtained from the same run as the images of Fig. 3. The flame leading tip is defined as in Ref. [51]. The flame tip along the axis of the duct is treated as the leading tip before inversion. The flame tip near the upper sidewall is the leading tip after inversion. The trajectories of flame leading tip locations versus time can be roughly divided into two stages: (1) an exponentially increasing stage, and (2) a slowly increasing stage. The flame leading tip location increases exponentially in time. It relates to the finger-shaped stage. Actually, as demonstrated in Fig. 2, the flame expands as a hemispherical

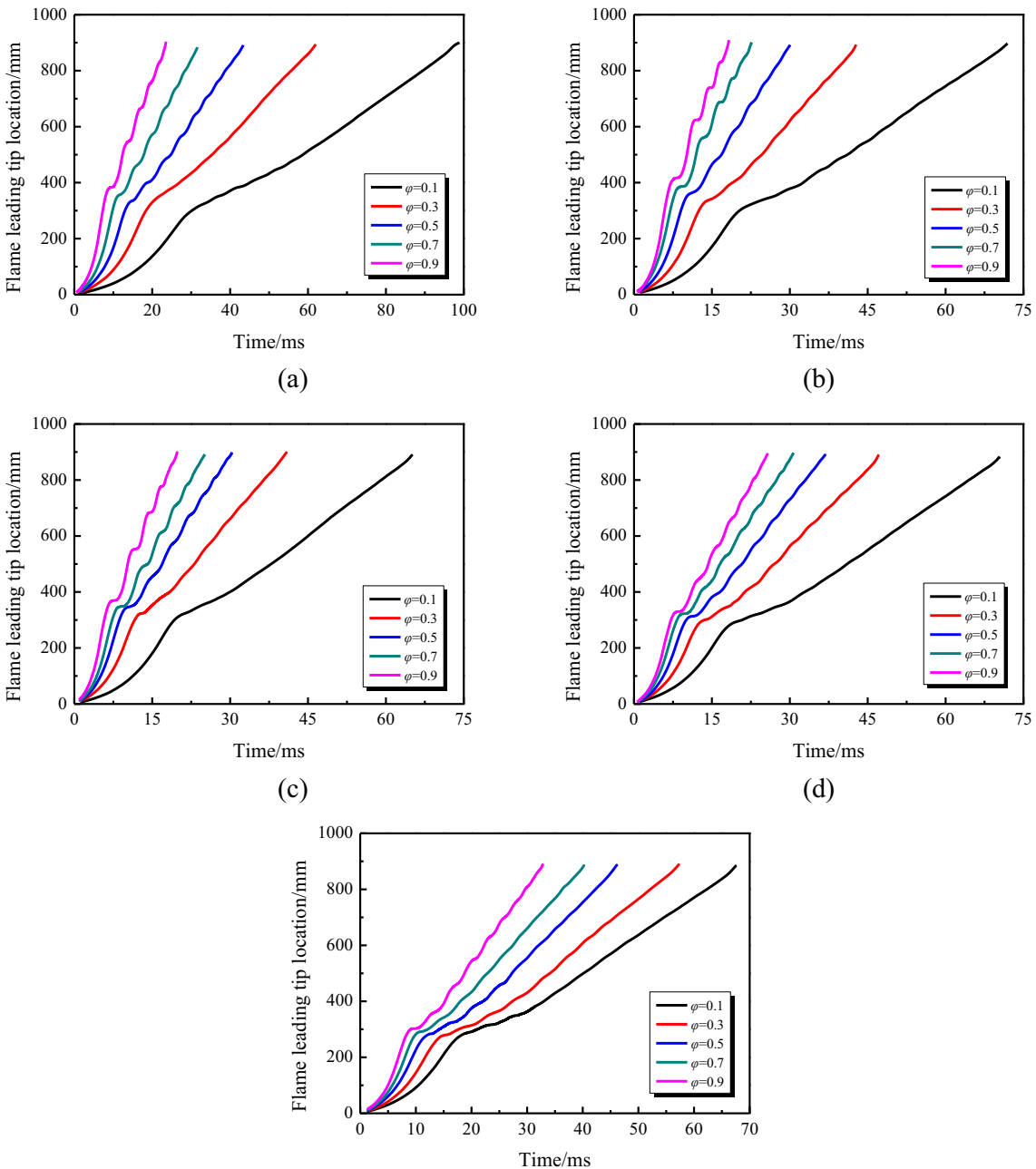


Fig. 4 – Flame leading tip location versus time at (a) $\Phi = 1.0$, (b) $\Phi = 1.5$, (c) $\Phi = 2.0$, (d) $\Phi = 2.5$, (e) $\Phi = 3.0$.

shape with laminar speed propagation after ignition. The location increases linearly in time, but the linear increases just maintain for a short time. Thus, the exponentially increasing stage includes two parts, i.e.: a short linear increase and an exponential increase. When the flame surface initially touches the sidewalls, the flame starts to invert. The flame propagates slowly as a tulip or distorted tulip shape, and the location increases slowly in time. The fluctuation relates to flame propagation with the tulip and distorted tulip flame shape interconversion.

The increase of the hydrogen fraction leads to a larger distance at the same time instant, as shown in Fig. 4. The time for flame arrival at the discharge vent decreases with the increase in the hydrogen fraction, especially for hydrogen

fractions between 0.1 and 0.3 (see the black and red trajectories in Fig. 4). Table 1 shows the time of flames reaching the discharge vent in all cases. For the same equivalence ratio, the difference of the flame propagation time between two adjacent hydrogen fractions decreases as the hydrogen fraction increases. The flame propagation time will decrease rapidly when the hydrogen fraction is between 0.1 and 0.3. For example, when the equivalence ratio is 1.0, it needs 98.89 ms for flame to arrive at the discharge vent with a hydrogen fraction of 0.1, whereas it will decrease to 62.00 ms with a hydrogen fraction of 0.3. The flame propagation time decreases approximately 36.89 ms, and the rate is approximately 37.30%. When the hydrogen fraction is larger than 0.5 ($\varphi \geq 0.5$), the flame propagation time will decrease moderately.

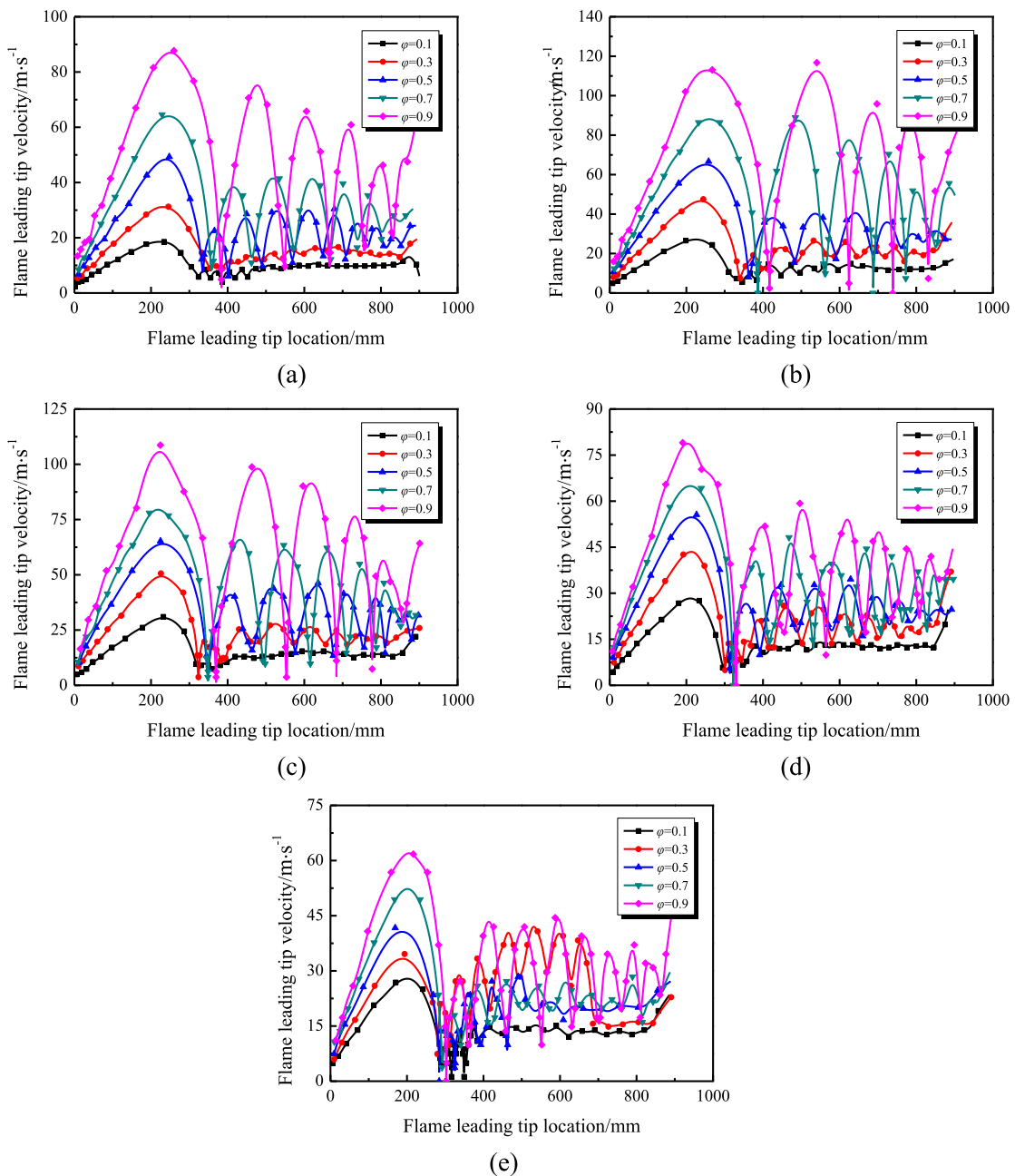


Fig. 5 – The relationship between flame leading tip velocity and location at (a) $\Phi = 1.0$, (b) $\Phi = 1.5$, (c) $\Phi = 2.0$, (d) $\Phi = 2.5$, (e) $\Phi = 3.0$.

Noticeably, the flame propagation time decreases gradually when the equivalence ratio is 3.0. This might be caused by unstable combustion in rich-fuel conditions as mentioned above. The equivalence ratio can affect the flame propagation time. When the hydrogen fraction is lower than 0.5 ($\phi < 0.5$), the minimum flame propagation time can be obtained at an equivalence ratio of 2.0; and when the hydrogen fraction is larger than 0.5 ($\phi \geq 0.5$), the minimum value will appear at an equivalence ratio of 1.5.

The formation of tulip and distorted tulip flames are always accompanied by a local flame velocity change [40,49]. Fig. 5 presents the flame leading tip velocity under various

Table 1 – Time for flame arrival at vent/ms.

Hydrogen fraction/ ϕ	Equivalence ratio/ ϕ				
	1.0	1.5	2.0	2.5	3.0
0.1	98.89	71.92	65.10	70.37	67.58
0.3	62.00	42.78	40.92	47.12	57.35
0.5	43.40	30.07	30.38	36.89	46.19
0.7	31.62	22.63	25.11	30.69	40.30
0.9	23.56	18.29	19.84	25.73	32.86

equivalence ratios and hydrogen fractions. The flame accelerates fast at the exponentially increasing stage as mentioned above, and as experimentally and analytically demonstrated in Refs. [28,50]. The flame accelerates more dramatically with the increase in the hydrogen fraction, as shown in Fig. 5. The acceleration terminates as the flame skirts initially touch the sidewalls and the flame surface area starts decreasing [50]. The flame deceleration stops as plane flame formation. The surface area changes with the tulip flame or the distorted tulip flame formation process. There are two kinds of flame leading tip velocity trajectories after tulip flame formation. The first is that the flame will continue propagating in this tulip shape to the vent with an approximate constant velocity. The distorted tulip flame propagation is always accompanied by flame leading tip velocity fluctuations [49], resulting in another flame velocity trajectory.

Apparently, the velocity fluctuation can be observed at all equivalence ratios with hydrogen fraction $\varphi \geq 0.5$, as shown in Fig. 5. It is difficult to identify the distorted tulip flame at an equivalence ratio of 1.0 and hydrogen fraction of 0.5 because of significant flame surface brightness, as shown in Fig. 3(a). The flame leading tip velocity, however, fluctuates with a near-constant amplitude (see the blue line in Fig. 5(a)). That amplitude indicates that the distorted tulip flame formed in this case. When the hydrogen fraction is 0.3, the prominent flame leading tip velocity fluctuation can be obtained at an equivalence ratio of 1.5 and above ($\varphi \geq 1.5$), (see the red line in Fig. 5). As mentioned above, the distorted tulip flame can be precisely identified at an equivalence ratio of $\varphi \geq 2.0$. For the equivalence ratio of 1.5 and hydrogen fraction of 0.3, the small cusp on the tulip flame lips results in flame leading tip velocity fluctuations, suggesting that distortion occurs in this case. For an equivalence ratio of 1.0 and hydrogen fraction of 0.3, there is no obvious tulip distortion after the tulip flame formation.

The flame propagation velocity will increase with the hydrogen fraction. Table 2 presents the maximum flame propagation velocity before inversion. The maximum flame propagation velocity is obtained at an equivalence ratio of 2.0 when the hydrogen fractions are 0.1 and 0.3, and the maximum value will be obtained at an equivalence ratio of 1.5 when the hydrogen fraction is $\varphi \geq 0.5$. The results are consistent with the flame propagation time. However, the difference of the maximum flame velocity between two adjacent hydrogen fractions is nearly the same. The maximum flame velocity is obtained before the surface touches the sidewalls. The laminar flame speed increases linearly with the hydrogen fraction [18]. After the flame touches the sidewalls, the interaction between the flame

surface and sidewalls can affect the flame propagation velocity. Moreover, the formation of the tulip and distorted tulip flames has a significant influence on the surface area, which can cause a significant discrepancy for the flame propagation times between two adjacent hydrogen fractions. The distortion becomes observable as the hydrogen fraction increases. Tulip distortion is closely connected with the maximum flame velocity. A pressure wave is generated as the flame touches the sidewalls [40]. The higher the flame propagation velocity is, the stronger the pressure waves generates. Tulip distortion is primarily caused by the interaction between the flame front and pressure waves [40]. In Fig. 5 and Table 2, the obvious flame speed oscillation can only be observed in cases where the maximum flame velocity is larger than 31.27 m s^{-1} . This means that the pressure waves that play a significant role in the appearance of tulip flame distortion can only be generated when the maximum flame velocity is larger than this value. Thus, the distorted tulip flame cannot be obtained in the cases of $v_{\max} \leq 31.27 \text{ m s}^{-1}$.

According to the recent research, the formation of the tulip flame is a purely hydrodynamic phenomenon [54], whereas the distorted tulip flame is initially caused by Rayleigh-Taylor instability [40,44]. The interaction between the flame front and pressure waves primarily creates the cusp on the tulip flame lips. Fig. 6 shows the relationship between overpressure and flame leading tip velocity in the propagation direction versus time at $\varphi = 1.0$, with $\varphi = 0.1$ and $\varphi = 1.0$, with $\varphi = 0.9$. Fig. 6(a) is the case of tulip flame propagation, and the distorted tulip flame is shown in Fig. 6(b). The venting pressure, defined as the first peak in the pressure signals [55], can be clearly distinguished in Fig. 6(a) (see the red line). The venting pressure is approximately 94.90 mbar. This pressure is required to break the PVC membrane on the discharge vent, and it will become inconspicuous with increasing hydrogen fraction because the overpressure will increase rapidly. The effect of the venting pressure on flame propagation can be neglected [41].

It can be seen from Fig. 6(a) that the overpressure trajectory can be divided into three stages. The first is that the overpressure increases simultaneously with the increase in flame leading tip velocity, but the increase will terminate at approximately $t_1 = 30.50 \text{ ms}$. In this stage, the overpressure increases rapidly because the flame surface area increases exponentially in time [50]. The overpressure decreases gradually with the observable pressure oscillation at the time between $t_1 = 30.40 \text{ ms}$ and $t_2 = 52.47 \text{ ms}$. Meanwhile, the flame front velocity fluctuates at this stage, but the amplitude is much smaller than that of the distorted tulip flame (compared with Fig. 6(b)). The fluctuation may be caused by pressure waves in the duct. The interaction between pressure waves and the flame front surface always accompanies flame propagation, and it will enhance flame acceleration, deceleration and deformation. However, the pressure waves are not strong enough to make the tulip flame distortion in this case. The pressure decrease can be explained by slow propagation velocity. The flame propagates very slowly with an average velocity of approximately 6.0 m/s. The volumetric flow rate through the discharge vent is slightly larger than the combustion rate. As a result, the overpressure decreases. For $t > 52.47 \text{ ms}$, the overpressure increases again, but very slowly.

Table 2 – Maximum flame propagation velocity before flame inversion $v_{\max}/\text{m s}^{-1}$.

Hydrogen fraction/ φ	Equivalence ratio/ φ				
	1.0	1.5	2.0	2.5	3.0
0.1	18.58	27.76	31.00	28.82	28.71
0.3	31.27	47.55	50.63	44.46	34.58
0.5	49.33	66.69	65.27	55.57	41.68
0.7	64.56	88.92	80.45	66.07	53.72
0.9	87.71	113.10	108.68	79.04	62.57

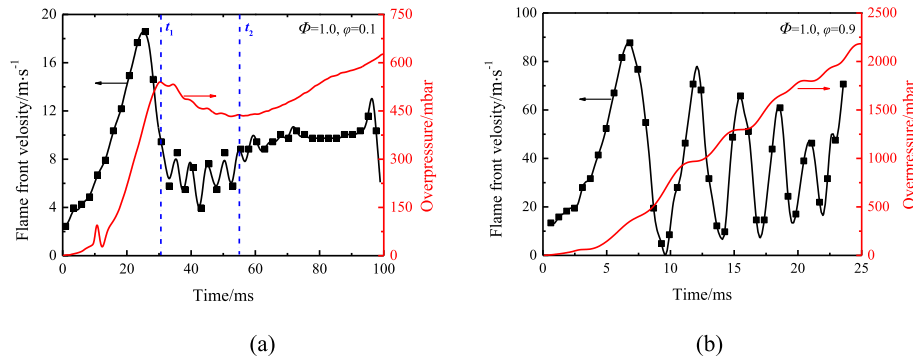


Fig. 6 – Relationship between pressure and flame leading tip velocity versus time. (a) $\Phi = 1.0$ of $\phi = 0.1$, (b) $\Phi = 1.0$ of $\phi = 0.9$.

The flame velocity increases to approximately 9.7 m/s in this stage. The volumetric flow rate through the discharge vent is slightly smaller than the combustion rate at this stage, and the overpressure reaches a maximum value when the flame leading tip arrives at the right end of the duct.

The distinguished pressure dynamic of the distorted tulip flame is shown in Fig. 6(b), and it is similar to the experimental and numerical results in Ref. [43]. The oscillation coincides well with the flame leading tip velocity fluctuation. Xiao et al. [40,44] suggest that Rayleigh-Taylor instability is the primary reason for tulip flame distortion. The distorted tulip flame can be obtained from premixed propane/air and acetylene/air flames at an equivalence ratio of 1.0 [47,49]. However, no obvious pressure dynamic oscillation appears during flame propagation. Shen and Duan [47,49] suggest that pressure waves enhance the distortion, but the distorted tulip flame is a consequence of multi-factor coupling, including the effects of the wall, boundary layer, squish flow, hydrodynamic instability and flame-induced flow. It is noteworthy that the overpressure oscillations exist in all distorted tulip flame cases that are observed in the present study. Actually, the pressure waves are initially created in the ignition process and are also generated when the flame skirts touch the sidewalls [40]. The pressure waves become stronger as the flame propagates. Absolutely, the interaction between pressure waves and the flame front plays an important role in distorted tulip flame formation.

Flame inversion and distortion

As analysed above, flame dynamics in a closed duct are closely connected with the hydrogen fraction in syngas mixtures at the later stage. There are four stages of tulip flames and an additional stage for a distorted tulip flame. The hydrogen fraction can affect the formation of each stage, especially the distorted stage. Both the geometrical model [28] and the analytical theory [50] indicate that tulip flame formation is affected by the laminar flame speed and the duct cross-section width. In addition, the expansion efficiency and flame instability also influence flame structure and shape.

In the present study, a classical tulip flame can be obtained in all cases, as shown in Fig. 3. The plane flame formation time is a critical parameter for characterizing the flame inversion, and the inversion time is conventionally referred to as the time of the plane flame. Fig. 7 shows the time t_{plane} when the

plane flame forms in the duct under various equivalence ratios and hydrogen fractions. The time t_{plane} changes with equivalence ratios. The change is significant for hydrogen fractions between 0.1 and 0.3, and it becomes smooth for hydrogen fractions larger than 0.5 ($\phi \geq 0.5$). The time, t_{plane} , decreases with the equivalence ratio increase when the hydrogen fraction is 0.1. The time decreases rapidly with a larger absolute slope when the equivalence ratio is between 1.0 and 1.5. The laminar flame speed increases dramatically for $\phi < 1.6$, and it increases moderately until the equivalence ratio approaches 3.0 [16,18]. The time t_{plane} decreases as the hydrogen fraction increases. Nevertheless, the time t_{plane} decreases rapidly for hydrogen fractions less than 0.5 ($\phi < 0.5$), and it will decrease moderately when the hydrogen fraction is larger than 0.5 ($\phi \geq 0.5$). The trajectory of plane formation time between two adjacent ratios decreases as the hydrogen fraction increases. The laminar flame speed will increase with the hydrogen fraction, and the increase varies with hydrogen fractions. Consequently, the time t_{plane} decrease is a different trend that is inversely proportional to the laminar flame speed.

As mentioned above, the distorted tulip flame can be distinguished at all equivalence ratios when $\phi \geq 0.5$, and the tulip distortion occurs at an equivalence ratio of 1.5 and above when $\phi = 0.3$. Following the geometrical model by Clanet and

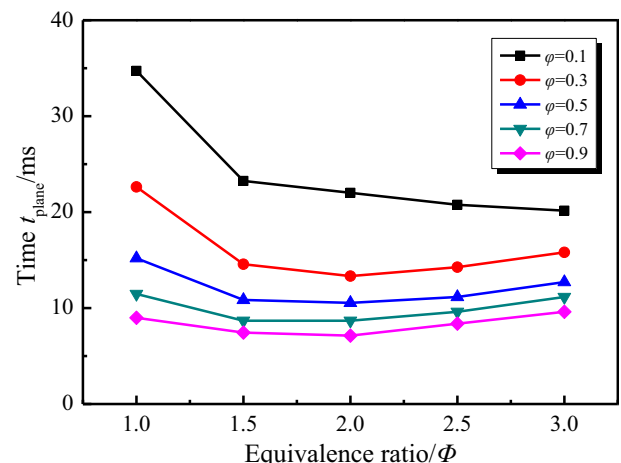


Fig. 7 – The plane flame formation time under various conditions.

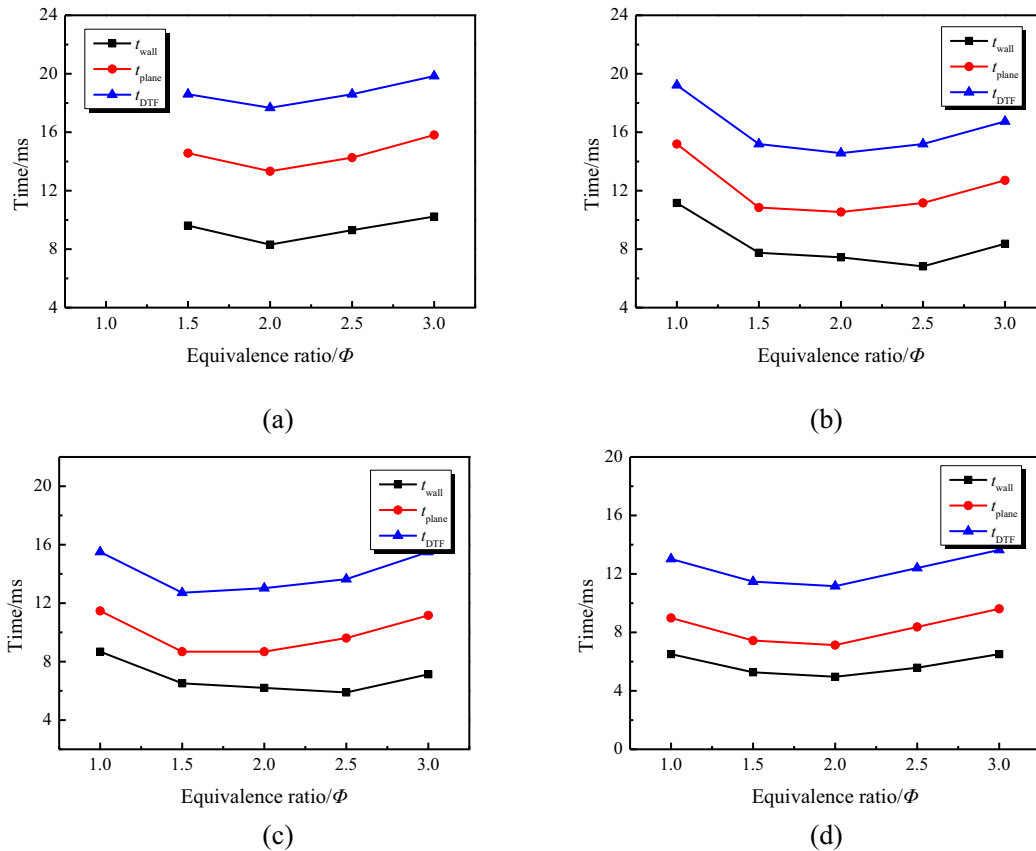


Fig. 8 – Relationship between initial flame inversion time and the initial first tulip distortion time under various equivalence ratios. (a) $\varphi = 0.3$, (b) $\varphi = 0.5$, (c) $\varphi = 0.7$, and (d) $\varphi = 0.9$.

Searby [28], the four phases of tulip flame formation can be expressed as follows: (1) the spherical flame stage, $t_0 < t < t_{\text{sphere}} = 0.1(R/U_L) \pm 0.02(R/U_L)$; (2) the finger flame stage, $t_{\text{sphere}} < t < t_{\text{wall}} = 0.26(R/U_L) \pm 0.02(R/U_L)$; (3) the flame inversion stage, $t_{\text{wall}} < t < t_{\text{tulip}} = 0.33(R/U_L) \pm 0.02(R/U_L)$; and the tulip flame $t_{\text{tulip}} < t$. The time instant of the plane flame formation is called t_{tulip} in Ref. [28]; thus, $t_{\text{tulip}} = t_{\text{plane}}$. Fig. 8 presents the relationship among the flame skirts touching the sidewalls initiation time, t_{wall} , the plane flame formation initiation time, t_{plane} , and the first tulip distortion initiation time, t_{DTF} , in a closed duct. The trajectories of t_{wall} , t_{plane} , and t_{DTF} share the same tendency at all equivalence ratios. The time interval between two adjacent stages decreases with the laminar flame speed increase, U_L , in the tulip flame formation process, e.g., the time interval between t_{plane} and t_{wall} is $0.07(R/U_L) \pm 0.02(R/U_L)$. Obviously, the vertical distance between the black and red trajectories in Fig. 8 varies with equivalence ratios and hydrogen fractions because of different laminar flame speed. However, the time interval between t_{plane} and t_{DTF} is nearly constant. Compared with the time interval between t_{plane} and t_{wall} , this constant does not change with the laminar flame speed U_L , and it is approximately 4.03 ms in the present study. Higher laminar flame speed results lower initial distortion time, but the interval between the initial first distortion and the plane flame is stationary. The interaction between the flame front surface and pressure waves is related to tulip flame distortion [40,44]. Therefore, it is rational to

propose that the interval time between the plane flame and the distorted tulip flame is constant.

Conclusions

The propagation of premixed syngas/air flames in a closed rectangular duct is investigated experimentally using a high-speed camera and pressure transducer. The flame structure, flame leading tip velocity and pressure dynamics are obtained. The influence of fuel composition and equivalence ratio on flame behaviour and propagation characteristics of the mixtures are also analysed. The main conclusions are summarized as follows:

- (1) A tulip flame forms in all equivalence ratios and hydrogen fractions. The distorted tulip flame forms in some cases: i.e., when the hydrogen fraction is $\varphi \geq 0.5$, a prominently distorted tulip flame can be produced after the full formation of a classical tulip flame at all equivalence ratios; and when $\varphi < 0.5$, the visible distortion only occurs at an equivalence ratio of 1.5 and above with $\varphi = 0.3$.
- (2) The syngas mixture hydrogen fraction has a significant influence on flame shape, propagation time, and velocity. The flame shape deformation, the formation of the tulip flame and the distorted tulip flame become

- observable as the hydrogen fraction increases. The flame propagation time of the syngas/air mixture decreases with the hydrogen fraction. When the hydrogen fraction is $\varphi \geq 0.5$, the minimum flame propagation time is obtained at $\Phi = 1.5$, whereas the minimum value will be acquired at $\Phi = 2.0$ when $\varphi < 0.5$.
- (3) The pressure dynamics are presented for both the tulip and distorted tulip flames. The influence of pressure on flame propagation is expressed as flame velocity. Distortion occurs when the maximum flame velocity is larger than 31.27 m s^{-1} , and the velocity fluctuates as the overpressure increases in a stepwise manner. The pressure waves play a dominant role in distorted tulip flame formation since the flame propagation occurred under the continuously increasing pressure created by the propagating front, and the interaction between the flame front and pressure waves results in tulip flame distortion.
- (4) The characteristic formation times of the plane flame and initial tulip distortion at different equivalence ratios and hydrogen fractions are also measured. The plane flame formation time is directly influenced by the laminar speed velocity. The initial distortion time and the plane flame formation time share a similar trend with all equivalence ratios. The interval between the plane flame formation time and the initial distortion time is constant at 4.03 ms in this work. This study may help build the quantitative theory or models for the distorted tulip flames in the future.

Acknowledgments

This research was funded by National Natural Science Foundation of China (No. 51774059, 51674104, 51574111, 51774115) and China Postdoctoral Science Foundation (No. 2018M631065).

REFERENCES

- [1] Liewen T, Yang V, Yetter R. *Synthesis gas combustion: fundamentals and applications*. CRC Press; 2009.
- [2] Salzano E, Basco A, Cammarota F, Di Sarli VV, Di Benedetto A. Explosions of syngas/CO₂ mixtures in oxygen-enriched air. *Ind Eng Chem Res* 2012;51(22):7671–8.
- [3] Toledo M, Araus K, Vasconcelo D. Syngas production from coal in presence of steam using filtration combustion. *Int J Hydrogen Energy* 2015;40:6340–5.
- [4] Sansaniwal SK, Rosen MA, Tyagi SK. Global challenges in the sustainable development of biomass gasification: an overview. *Renew Sustain Energy Rev* 2017;80:23–43.
- [5] Caro S, Torres D, Toledo M. Syngas production from residual biomass of forestry and cereal plantations using hybrid filtration combustion. *Int J Hydrogen Energy* 2015;40:2568–77.
- [6] He MY, Xiao B, Liu SM, Hu ZQ, Luo SY, Yang F. Syngas production from pyrolysis of municipal solid waste (MSW) with dolomite as downstream catalysts. *J Anal Appl Pyrol* 2010;87(2):181–7.
- [7] He D, Yan WP. Influences of different diluents on NO emission characteristics of syngas opposed-flow flame. *Int J Hydrogen Energy* 2018;48(5):2570–84.
- [8] Fu J, Tang CL, Jin W, Dinh Thi L, Huang ZH, Zhang Y. Study on laminar flame speed and flame structure of syngas with varied compositions using OH-PLIF and spectrograph. *Int J Hydrogen Energy* 2013;38(3):1636–43.
- [9] Tran MV, Scribano G, Cheng TC, Ho TX, Huynh TC. Experimental and numerical investigation of explosive behavior of syngas/air mixtures. *Int J Hydrogen Energy* 2018;43(16):8152–60.
- [10] Tran MV, Scribano G, Cheng TC, Ho TX. Influence of hydrocarbon additions and dilutions on explosion behavior of syngas/air mixtures. *Int J Hydrogen Energy* 2017;42(44):27416–27.
- [11] Xie YL, Wang JH, Cai X, Huang ZH. Pressure history in the explosion of moist syngas/air mixtures. *Fuel* 2016;85:18–25.
- [12] Askari O, Wang ZY, Vien K, Sirio M, Metghalchi H. On the flame stability and laminar burning speeds of syngas/O₂/He premixed flame. *Fuel* 2017;190:90–103.
- [13] Askari O, Moghaddas A, Alholm A, Vien K, Alhazmi B, Metghalchi H. Laminar burning speed measurement and flame instability study of H₂/CO/air mixtures at high temperatures and pressures using a novel multi-shell model. *Combust Flame* 2016;168:20–31.
- [14] Ai YH, Zhou Z, Chen Z, Kong WJ. Laminar flame speed and Markstein length of syngas at normal and elevated pressures and temperatures. *Fuel* 2014;137:339–45.
- [15] Zhang Y, Shen WF, Fan M, Zhang H, Li SH. Laminar flame speed studies of lean premixed H₂/CO/air flames. *Combust Flame* 2014;61(10):2492–5.
- [16] Bouvet N, Chauveau C, Gökalp I, Halter F. Experimental studies of the fundamental flame speeds of syngas (H₂/CO)/air mixtures. *Proc Combust Inst* 2011;33(1):913–20.
- [17] Bouvet N, Chauveau C, Gökalp I, Lee S-Y, Santoro RJ. Characterization of syngas laminar flames using the Bunsen burner configuration. *Int J Hydrogen Energy* 2011;36(1):992–1005.
- [18] Dong C, Zhou QL, Zhao QX, Zhang YQ, Xu TM, Hui SE. Experimental study on the laminar flame speed of hydrogen/carbon monoxide/air mixtures. *Fuel* 2009;88(10):1158–63.
- [19] Krejci MC, Mathieu O, Vissotski AJ, Ravi S, Sikes TG, Petersen E. Laminar flame speed and ignition delay time data for the kinetic modeling of hydrogen and syngas fuel blends. *J Eng Gas Turbines Power* 2013;135(02):1503–9.
- [20] Pang GA, Davidson DF, Hanson RK. Experimental study and modeling of shock tube ignition delay times for hydrogen–oxygen–argon mixtures at low temperatures. *Proc Combust Inst* 2009;32(1):181–8.
- [21] Zhang Y, Shen WF, Zhang H, Wu YX, Lu JF. Effects of inert dilution on the propagation and extinction of lean premixed syngas/air flames. *Fuel* 2015;157(1):115–21.
- [22] Zhang Y, Qiu XL, Li B, Zhang H, Li SH. Extinction studies of near-limit lean premixed syngas/air flames. *Int J Hydrogen Energy* 2013;38(36):16453–62.
- [23] Matalon M. Flame dynamics. *Proc Combust Inst* 2009;32:57–82.
- [24] Bychkov VV, Liberman MA. Dynamics and stability of premixed flames. *Phys Rep* 2000;325:115–237.
- [25] Ellis OCde C. Flame movement in gaseous explosive mixtures. *Fuel Sci* 1928;7:502–8.
- [26] Salamandra GD, Bazhenova TV, Naboko IM. Formation of detonation wave during combustion of gas in combustion tube. *Proc Combust Inst* 1959;7(1):851–5.
- [27] Dunn-Rankin D, Sawyer RF. Tulip flames: changes in shape of premixed flames propagating in closed tubes. *Exp Fluid* 1998;24:130–40.

- [28] Clenet C, Searby G. On the “tulip flame” phenomenon. *Combust Flame* 1996;105(1–2):225–38.
- [29] Dold J, Joulin G. An evolution equation modeling inversion of tulip flames. *Combust Flame* 1995;100:450–6.
- [30] Marra FS, Continillo G. Numerical study of premixed laminar flame propagation in a closed tube with a full Navier-Stokes approach. *Proc Combust Inst* 1996;26:907–13.
- [31] Xiao H, Wang Q, He X, Sun J, Yao L. Experimental and numerical study on premixed hydrogen/air flame propagation in a horizontal rectangular closed duct. *Int J Hydrogen Energy* 2010;35:1367–76.
- [32] Metzener P, Matalon M. Premixed flames in closed cylindrical tubes. *Combust Theor Model* 2001;5:463–83.
- [33] Matalon M, Metzener P. The propagation of premixed flames in closed tubes. *J Fluid Mech* 1997;336:331–50.
- [34] Markstein GH. A shock-tube study of flame front-pressure wave interaction. *Proc Combust Inst* 1959;6(1):387–98.
- [35] Dold JW, Joulin G. An evolution equation modeling inversion of tulip flames. *Combust Flame* 1995;100(3):450–6.
- [36] Matalon M, McGreevy JL. The initial development of a tulip flame. *Proc Combust Inst* 1994;25(1):1407–13.
- [37] Nkonga B, Fernandez G, Guillard H, Larrouetou B. Numerical investigations of the tulip flame instability—comparisons with experimental results. *Combust Sci Technol* 1993;87:69–89.
- [38] Gonzalez M, Borghi R, Saouab A. Interaction of a flame front with its self-generated flow in an enclosure: the “tulip flame” phenomenon. *Combust Flame* 1992;88(2):201–20.
- [39] Starke R, Roth P. An experimental investigation of flame behavior during cylindrical vessel explosions. *Combust Flame* 1986;66(3):249–59.
- [40] Xiao H, Houim RW, Oran ES. Formation and evolution of distorted tulip flames. *Combust Flame* 2015;162:4084–101.
- [41] Yu MG, Zheng K, Zheng LG, Chu TX, Guo PK. Scale effects on premixed flame propagation of hydrogen/methane deflagration. *Int J Hydrogen Energy* 2015;40:13121–33.
- [42] Xiao HH, Wang QS, Shen XB, Guo S, Sun JH. An experimental study of distorted tulip flame formation in a closed duct. *Combust Flame* 2013;160(9):1725–8.
- [43] Xiao HH, Makarov D, Sun JH, Molkov V. Experimental and numerical investigation of premixed flame propagation with distorted tulip shape in a closed duct. *Combust Flame* 2012;159:1523–38.
- [44] Xiao HH, Houim RW, Oran ES. Effects of pressure waves on the stability of flames propagating in tubes. *Proc Combust Inst* 2017;36(1):1577–83.
- [45] Xiao HH, Duan QL, Sun JH. Premixed flame propagation in hydrogen explosions. *Renew Sustain Energy Rev* 2017;81:1988–2001.
- [46] Zheng K, Yu MG, Liang YP, Zheng LG, Wen XP. Large eddy simulation of premixed hydrogen/methane/air flame propagation in a closed duct. *Int J Hydrogen Energy* 2018;43(7):3871–84.
- [47] Jin KQ, Duan QL, Liew KM, Peng ZJ, Gong L, Sun JH. Experimental study on a comparison of typical premixed combustible gas-air flame propagation in a horizontal rectangular closed duct. *J Hazard Mater* 2017;327:116–26.
- [48] Zheng K, Yu MG, Zheng LG, Wen XP, Chu TX, Wang L. Experimental study on premixed flame propagation of hydrogen/methane/air deflagration in closed ducts. *Int J Hydrogen Energy* 2016;42(8):5426–38.
- [49] Shen XB, He XC, Sun JH. A comparative study on premixed hydrogen-air and propane-air flame propagations with tulip distortion in a closed duct. *Fuel* 2015;161:248–53.
- [50] Bychkov V, Akkerman V, Fru G, Petchenko A, Eriksson LE. Flame acceleration in the early stages of burning in tubes. *Combust Flame* 2007;150(4):263–76.
- [51] Xiao HH, Wang QS, He XC, Sun JH, Shen XB. Experimental study on the behaviors and shape changes of premixed hydrogen-air flames propagating in horizontal duct. *Int J Hydrogen Energy* 2011;36(10):6325–36.
- [52] Xiao HH, Sun JH, Chen P. Experimental and numerical study of premixed hydrogen/air flame propagating in a combustion chamber. *J Hazard Mater* 2014;268(3):132–9.
- [53] Chaos M, Dryer FL. Syngas combustion kinetics and applications. *Combust Sci Technol* 2008;180(6):1053–96.
- [54] Ponizy B, Claverie A, Veysièvre B. Tulip flame – the mechanism of flame front inversion. *Combust Flame* 2014;161(12):3051–62.
- [55] Ibrahim SS, Masri AR. The effects of obstructions on overpressure resulting from premixed flame deflagration. *J Loss Prev Process* 2001;14(3):213–21.